Optimization of photocurrent in bulk heterojunction organic solar cells using optical admittance analysis method

Ompong, David; Narayan, Monishka; Singh, Jai

Published in:
Journal of Materials Science: Materials in Electronics

DOI:
10.1007/s10854-017-6491-8

Published: 01/05/2017

Document Version
Publisher's PDF, also known as Version of record

Optimization of Photocurrent in Bulk Heterojunction Organic Solar Cells using Optical Admittance Analysis Method

David Ompong , Monishka Narayan, and Jai Singh

School of Engineering and IT, B- Purple 12
Charles Darwin University, Darwin, NT 0909, Australia

Corresponding author email: jai.singh@cdu.edu.au

Abstract

The optimized thicknesses of the active individual layers in organic thin film solar cells are obtained using optical admittance analysis method (OAAM). We have used OAAM to simulate the optical properties of two bulk-heterojunction (BHJ) organic solar cells (OSCs) of structures: (1) ITO/PEDOT:PSS /P3HT:PCBM/Lif/Al and (2) ITO/PTB7:PCBM /Lif /Ag. The optimal thicknesses of 75 nm and 115 nm of P3HT:PCBM and PTB7:PCBM blend layers, respectively, are obtained by maximising the absorbance in these layers through this simulation, which agree very well with the experimental results. The simulated short-circuit current density(J_{sc}) is plotted as a function of the active layer thickness for a few selected thicknesses of the Al cathode in these two OSCs and it is found that J_{sc} becomes maximum when the thickness of Al cathode is 40 nm. Using these optimised thicknesses of the active layers in these two cells the short-circuit current density is found to increase in ITO/PEDOT:PSS/P3HT:PCBM/Lif/Al BHJ OSC by 4.8% and in ITO/PTB7:PCBM /Lif /Ag by 13.3% .

1. Introduction

Organic solar cells (OSCs) represent the next generation photovoltaics (PV) and they offer a wide range of novel and unconventional benefits such as integration into buildings and other devices, in addition to being of low cost, light weight, mechanically flexible and perhaps most important of all, having room temperature solution processed fabrication techniques[1-4]. With these attractive features, OSCs may be regarded to have a huge potential to compete with or even replace the current inorganic solar cells. The interest in OSCs for the last two decades has spurred extensive research effort around the globe to understand and improve the performance of these cells [5, 6]. The bulk heterojunction (BHJ) OSCs in which the organic donor and acceptor (D-A) blend creates nanoscale interconnected neat and mixed phases have produced high power conversion efficiency (PCE) and hence are currently the preferred device structure for further investigations [7-9].

In BHJ OSCs a thinner active layer thickness is desirable for efficient charge extraction, reduced charge carrier recombination, and minimum material cost, but then this occurs at the expense of reduced light absorption which increases with increase in layer thickness. Although the extinction coefficients of organic semiconductors can be more than a magnitude higher than that of inorganic semiconductors such as silicon, the low charge carrier mobilities in organic solids present a transport limitation in OSCs [10, 11]. In other words, due to the low charge carrier mobilities in organic semiconductors, the optimal active layer thickness is always a compromise between the photon absorption and charge carrier collection. For this reason light trapping schemes are very important in designing efficient organic and hybrid-organic solar cells [12, 13]. However, OSCs have thin active layers comparable to the coherence length of the incident light so their optical properties are substantially influenced by interference effects that contribute to the electromagnetic field modulation inside the device, such that absorption due to interference effects can sometimes dominate over that due to increased optical path length where diffraction grating is used [4, 14]. Since most of the solar energy is concentrated in the visible and near-infrared (IR) regions, OSCs designed to efficiently harvest solar energy must have a large overlap between its absorption spectra and

the solar spectrum. Efficient absorption in the whole solar spectrum should be the first design rule if the total efficiency of the solar cells is to improve [5]. Recent achievements in highly efficient thin film single-junction polymer solar cells are mainly based on advances in light manipulation schemes capable of enhancing photon absorption and thus exciton generation in the solar cells [15].

The traditional light trapping schemes, where one applies additional anti-reflection coating or texturing the surface of a thick conventional solar cell to redirect and trap light by total internal reflection (TIR), have limited applications in OSCs. These structures are relatively too large to employ on OSCs [11], of thicknesses in the 20-200 nm range [14]. It may also be noted that in such thin OSCs, less than 80 percent of the overall incident light is ultimately used in generating photocurrent [15]. As the thickness of an OSC is comparable to the wavelength of the incident light, and metal electrodes create highly reflecting interface thus coherent optics and wave effects which exploit the optical interference effects to aid absorption play a significant role in determining the optical properties of OSCs [11, 14].

In this work, we have selected two BHJ OSCs of structures: (1) ITO(180 nm)/PEDOT:PSS (45 nm)/P3HT:PCBM (1:1)(d nm)/Lif (1 nm)/Al (100 nm) and (2) ITO(100 nm)/PTB7:PCBM (1:1.5)(d nm)/Lif (15 nm)/Ag (100 nm) to optimize the active layer thicknesses by maximising the absorbance using optical admittance analysis method (OAAM). MATLAB environment is used for writing the computer simulation code. The optical properties of the OSCs are considered in the solar spectral wavelength range 300 nm to 900 nm in this modelling, optical isotropy of the D-A blend, and normal incidents of light are assumed throughout this work. The short-circuit current density (J_{sc}) is calculated at the standard AM 1.5 [16]. The thickness dependence of the J_{sc} thus calculated is compared with experimental data. The interference effects on J_{sc} at various interfaces of the layered structure are also studied.

2. Theory of the modelling

It is well established that in the propagation of an electromagnetic (EM) wave, the electric $(\vec{E})$ and magnetic $(\vec{H})$ field components, and unit vector $(\vec{s})$ in the direction of propagation are mutually perpendicular to each other and can be expressed as [17, 18]:

$$\vec{H} = y(\vec{s} \times \vec{E}) \tag{1}$$

where y is the admittance of the medium. For the propagation of an EM wave in a structure shown schematically in Fig. 1(a), the tangential components of the electric and magnetic fields at a boundary are assumed to be continuous across the boundary because there is no mechanism that will change their values. The magnitudes of the tangential electric and magnetic components at two successive boundaries will defer in phase by a factor due to the optical path difference. Thus the fields between two interfaces are always related by a phase difference. Consider an organic solar cell that has *m* layers deposited on a substrate as the *(m+1)th* layer of the whole structure. Following the procedure of OAAM given in [18, 19], the thin film layers of the solar cell as shown in Fig. 1(a) are reduced to a single layer with interfaces (*a*) and (*b*) as shown in Fig. 1(b). The effective optical admittance (y_{eff}) of this multilayer structure can be written as [18, 19]:

$$y_{eff} = C/B \tag{2}$$

where *B* and *C* are obtained from the characteristic matrix equation [17]:

$$\begin{bmatrix} B \\ C \end{bmatrix} = \prod_{j=1}^{m} \left\{ \begin{bmatrix} \cos\delta_j & \frac{i\sin\delta_j}{y_j} \\ iy_j \sin\delta_j & \cos\delta_j \end{bmatrix} \right\} \begin{bmatrix} 1 \\ y_{m+1} \end{bmatrix} \tag{3}$$

where y_j and y_{m+1} are the optical admittance of the *j*th layer and substrate, respectively, and δ_j is the phase difference given by:

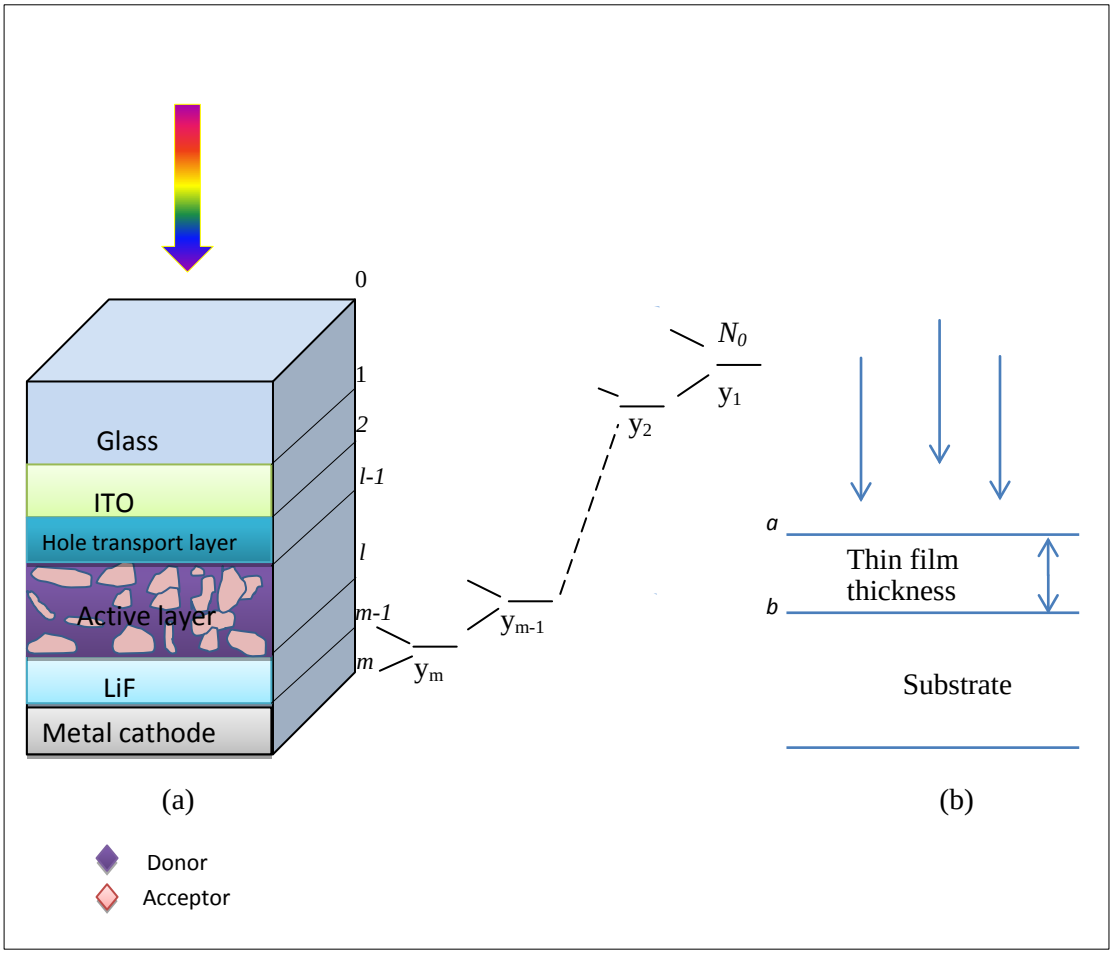

Fig. 1a. Solar cell structure used in this study

Fig. 1 b. Schematic diagram of a plane wave incident on a thin film

$$\delta_j = \frac{2\pi d_j}{\lambda} N_j \cos\theta \tag{4}$$

Here d_j is the thickness of the jth layer, $N_j = n_j + ik_j$ is the corresponding complex refractive index as a function of the wavelength λ, of the incident light, n_j is the refractive index, k_j is the extinction coefficient, and θ is the angle of refraction on the top interface of the *jth* layer. The optical admittance of the substrate is given as:

$$y_{m+1} = N_s y^o \tag{5}$$

where N_s is the complex refractive index of the substrate and $y^o = \frac{1}{377}$[Siemens] is the admittance of vacuum. Using y_{eff} in Eq. (2) one can calculate the total reflectance from the whole structure as:

$$R(\lambda) = \left| \frac{y_{air} - y_{eff}}{y_{air} + y_{eff}} \right|^2 \quad (6)$$

where y_{air} is the optical admittance of air. For a non-absorbing dielectric assembly, the transmittance is $T(\lambda) = [1 - R(\lambda)]$ but for an assembly containing both absorbing and non-absorbing layer, subsidiary calculations involving the ratio of the output to the input irradiances are necessary, this gives the total transmittance in the case of absorption as [17]:

$$T(\lambda) = [1 - R(\lambda)] \prod_{j=1}^{m} \psi_j \quad (7)$$

where ψ_j is the ratio of the time average numerical magnitude of the Poynting's vector at the *j*th and the (*j+1)*th boundaries[18, 20] given by:

$$\psi_j = \frac{\mathrm{Re}(y_{j+1})}{\mathrm{Re}(y_j) \left| \cos\delta_j + y_{j+1} \frac{\sin\delta_j}{N_j} \right|^2} \quad (8)$$

where $\mathrm{Re}(y_j)$ and $\mathrm{Re}(y_{j+1})$ represent the real part of the effective admittance for *j*th and the (*j+1)*th layers, respectively. Thus, the total absorbance of the multilayer system can be obtained as:

$$A(\lambda) = 1 - T(\lambda) - R(\lambda) \quad (9)$$

However, in most cases we are not interested in the total absorbance of the whole structure, like the solar cell, we require only the absorbance in a particular layer which generates photocurrent. For calculating the absorbance in the *l*th layer Eq. (10) is used as [17, 18]:

$$A_l(\lambda) = [1 - R(\lambda)][1 - \psi_i(\lambda)] \prod_{j=1}^{i-1} \psi_j \quad (10)$$

J_{sc} is obtained as a function of the layer thickness by integrating the product of the absorbance in Eq. (10) and the photon flux at AM1.5 over 300–900 nm spectral range [21] as:

$$J_{sc} = q \int_{\lambda} A_l(\lambda) \Phi(\lambda) d\lambda \quad (11)$$

here $\Phi(\lambda)$ is the spectral density of the photon irradiance, q is electron charge, A_l is the active layer absorbance which is a dimensionless wavelength dependent number between zero and one. J_{sc} in Eq. (11) can be optimized with respect to the layer thickness.

3. Results

We have used OAAM thus developed here for studying the following two BHJ OSCs of: 1) poly(3-hexylthiophene):1-(3-methoxycarbonyl)-propyl-1-phenyl-(6,6)C (P3TH:PCBM) and 2) poly[[4,8-bis[(2-ethylhexyl)oxy]benzo[1,2-b:4,5-b']dithiophene-2,6-diyl][3-fluoro-2-(2-ethylhexy) carbonyl] thieno [3,4-b] thiophenediyl]]):1-(3-methoxycarbonyl)-propyl-1-phenyl-(6,6)C (PTB7:PCBM) blends. The complex refractive index of the material and the thickness of each layer are needed in the modeling. The sources of the complex refractive indices taken from the library of SETFOS software are; Lithium Floride (Lif), and

Silver (Ag) [22], indium tin oxide (ITO), and aluminum (Al) [23], P3TH:PCBM blend [24]. The optical constants for poly[3,4-(ethylenedioxy) thiophene]: poly(styrene sulfonate) (PEDOT:PSS), and PTB7:PCBM are from [25].

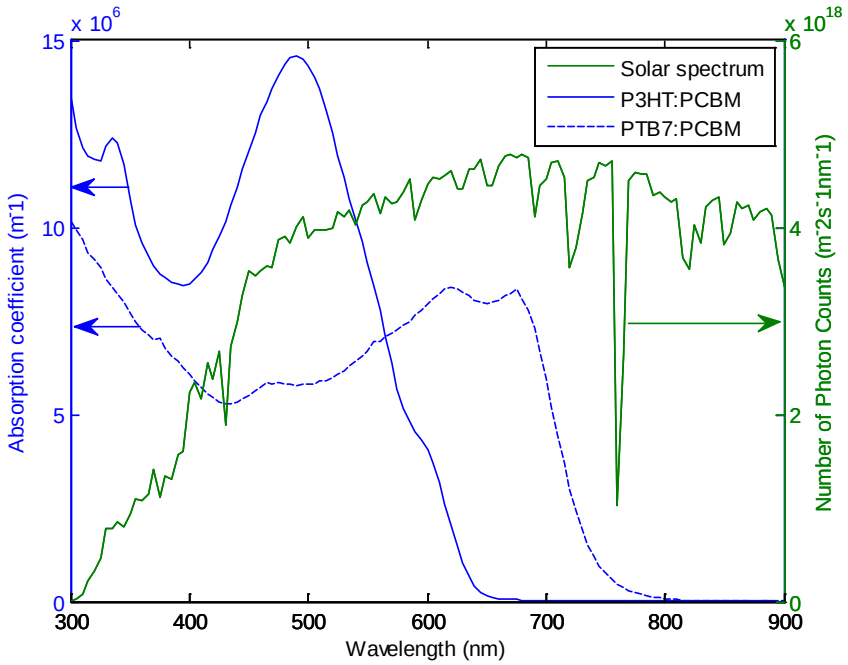

Fig. 2. Absorption coefficients of P3TH:PCBM (blue solid line) and PTB7:PCBM (blue dash line) blends overlaid with the photon flux of AM 1.5 solar spectrum (green solid line), given in the form of number of photon counts, as shown on the right axis

The amount of light absorbed in the active layer of a solar cell depends mainly on the (*n*, *k*) values of the material, the optical path length of light inside the layer, and interference effects, if any. Also, an efficient absorbing layer should have an absorption spectrum that overlaps reasonably well with the solar spectrum in the visible and near infrared regions [5]. The absorption coefficient is calculated using $\alpha = 4\pi k / \lambda$for P3TH:PCBM (blue solid line) and PTB7:PCBM (blue dash line) blends and photon flux at AM 1.5 of solar spectrum (green solid line) and plotted in Fig.2 as a function of radaition wavelength. According to Fig. 2, the PTB7:PCBM system has a wider overlap with the solar spectrum between 400 to 720 nm.

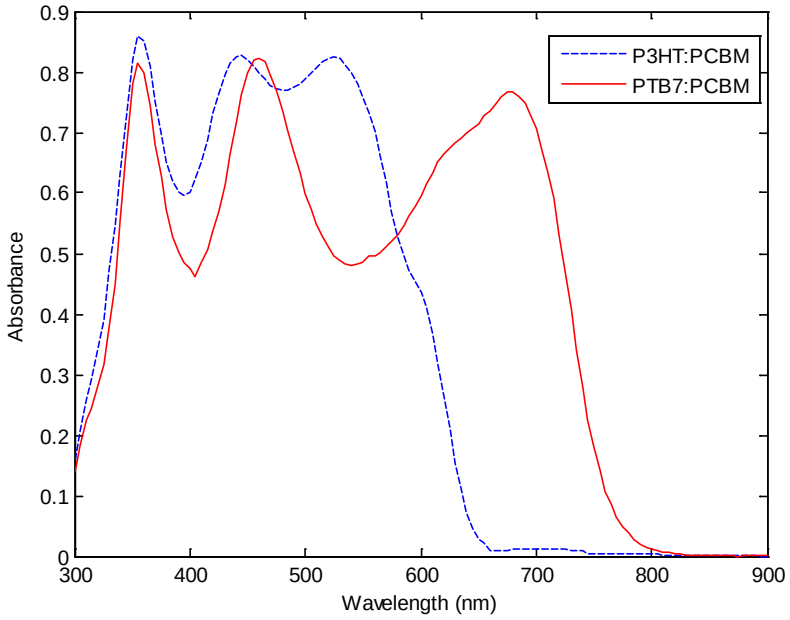

Fig. 3. Absorbance of P3TH:PCBM (red solid line) and PTB7:PCBM (blue dash line) blends versus wavelength of light

The calculated absorbance using Eq. (10) for the active layers P3TH:PCBM and PTB7:PCBM, each of 75 nm thick, is shown in Fig.3 as a function of the wavelength. Absorption in the other layers of the assembly is not considered as it does not contribute to the photocurrent. The characteristic matrix Eq. (3) in OAAM takes into account multiple reflections within the layers [18] and subsequent interference effects [26] and hence the results obtained are expected to be more accurate than those obtained from the traditional Beer-Lambert law.

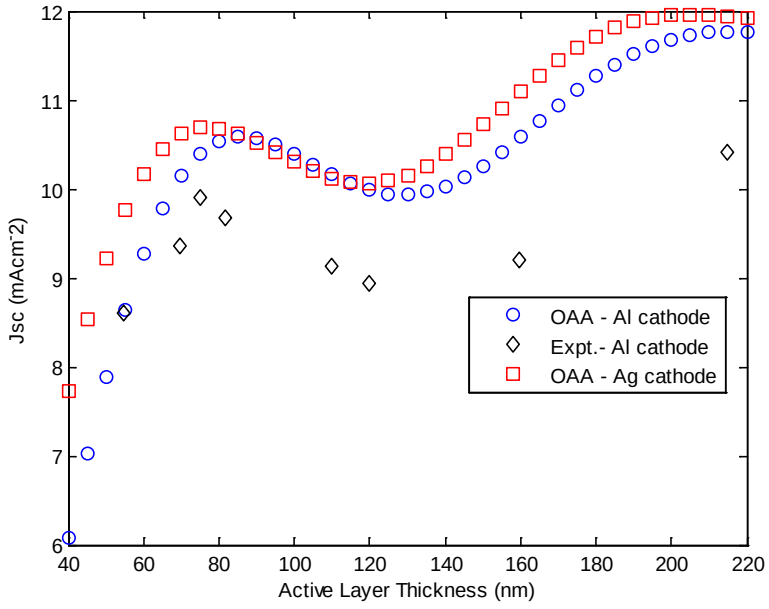

Fig. 4. J_{sc} of P3HT:PCBM blend as a function of blend thickness modeled using OAAM with Al cathode (blue circles), Ag cathode (red squares) and experimental data (black diamonds) extracted from Monestier *et al*. [24].

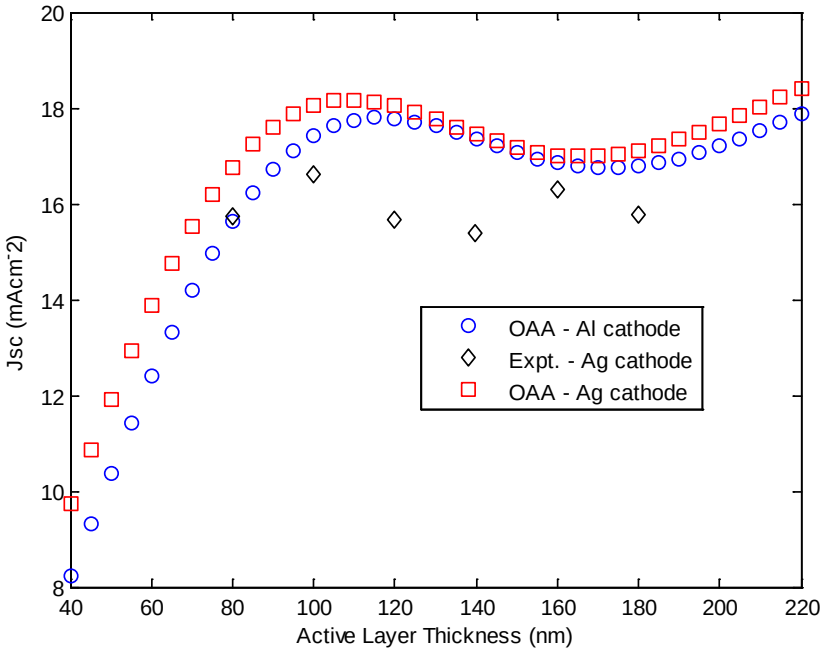

Fig. 5. J_{sc} of PTB7:PCBM blend as a function of blend thickness modeled using OAAM with Al cathode (blue circles), Ag cathode (red squares) and experimental data (black diamonds) extracted from Zheng *et al* [27].

Using Eq. (11), we have plotted J_{sc} as a function of the active layer thickness for P3TH:PCBM blend as shown in Fig.4 and in Fig. 5 for PTB7:PCBM blend. From Figs. 4 and 5, the optimum active layer thicknesses required for producing maximum photocurrent in the blends can be extracted. For the blends P3TH:PCBM (Fig. 4) and PTB7:PCBM (Fig. 5), the optimal thicknesses are obtained as 75 nm and 115 nm, respectively. The calculated J_{sc} as a function of the active layer thickness, d , of both OSCs is listed in Table 1, along with the corresponding experimental values.

Table 1: Calculated J_{sc} as a functio of the active layer thickness, d , and the corresponding experimental J_{sc} for the two BHJ OSCs

ITO/PEDOT:PSS/P3HT:PCBM/Lif/Al			ITO/PTB7:PCBM/Lif/Ag		
d/nm	Theoretical J_{sc}	Experimental J_{sc}[24]	d/nm	Theoretical J_{sc}	Experimental J_{sc}[27]
55	8.65	8.61	80	16.76	15.72
70	10.14	9.36	100	18.05	16.6
75	10.39	9.91	120	18.04	15.66
82	10.53	9.67	140	17.44	15.4
110	10.16	9.13	160	17.02	16.29
120	9.99	8.93	180	17.12	15.77
160	10.58	9.21			
215	11.77	10.41			

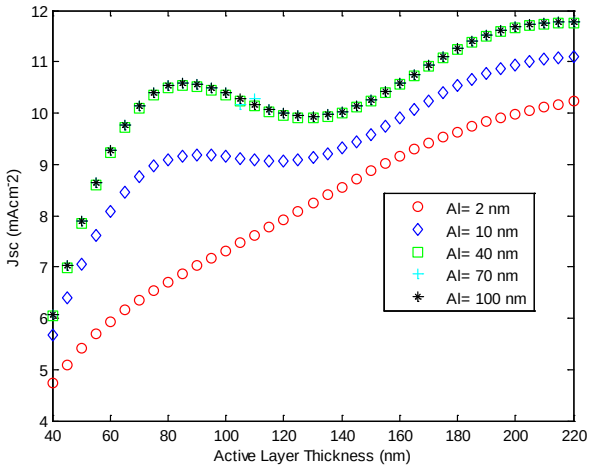

Fig. 6a. J_{sc} of P3HT:PCBM blend as a function of blend thickness with varying thickness of the aluminum metal cathode modeled using OAAM

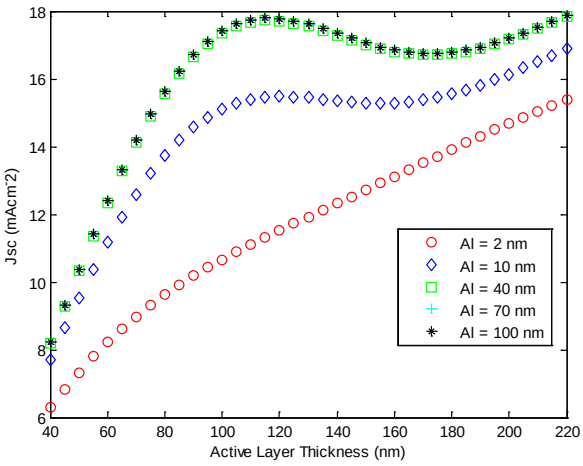

Fig. 6b. J_{sc} of PTB7:PCBM blend as a function of blend thickness with varying thickness of the aluminum metal cathode modeled using OAAM

The oscillatory behaviour of the J_{sc} as a function of thickness is indicative of interference effect. Strong interference effect is expected in a device with a thicker metal cathode like Al, because the metal acts as a reflector for the unabsorbed light in the active layer and reflects it back into the active layer for re-absorption [11]. For studying the influence of thickness of the cathode on the absorption, we have plotted J_{sc} as a function of the thickness of the active layer at five different thicknesses, 2, 10, 40, 70 and 100 nm of Al cathode as shown in Figs. 6 (a) and (b) for P3TH:PCBM and PTB7:PCBM blends, respectively. It can be clearly seen in Figs. 6 (a) and (b) that the interference effect becomes pronounced as the thickness of the Al electrode is increased. When the Al thickness is only 2 nm, the oscillations in the curves disappear in both OSCs, this can be attributed to the fact that, 2nm is not thick enough to create the interference due to the re-absorption effects in the active layer.

4. Discussion

We have applied optical admittance analysis method (OAAM) for simulating the short-circuit current density in BHJ OSCs. In particular, we have considered two BHJ OSCs of structures: (1) ITO(180 nm)/PEDOT:PSS (45 nm)/P3HT:PCBM (1:1)(d nm)/Lif (1 nm)/Al (100 nm) [24] and (2) ITO(100 nm)/PTB7:PCBM (1:1.5)(d nm)/Lif (15 nm)/Ag (100 nm) [27] so that we can compare the calculated results with the experimental ones. It should however be noted that in our simulation in Fig. 5, we have used ITO and LiF in place of ITO/ZnO and MoO_3 used in [27]. First we have studied the effect of overlap of solar radiation with the absorption coefficient in the two BHJ OSCs as shown in Fig. 2. Then the absorbance in the active layer of each OSC is calculated as shown in Fig. 3. In Fig. 2, we can see that PTB7:PCBM has a wider overlap between its absorption coefficient and the solar spectrum in the 400 to 720 nm wavelength range compared to P3HT:PCBM which has overlap only in the 560 nm to 650 nm range. This is consistent with the broad absorbance in PTB7:PCBM in the visible region in comparison with the narrower absorbance in P3HT:PCBM, as shown in Fig. 3. As a result, the former blend produces a higher J_{sc} than the latter one as discussed below.

It may also be noted that both blends do not have their absorption coefficients overlapping with the solar spectrum between 300 to 400 nm in Fig. 2, thus one may expect only a small contribution to the

absorbance in this range from both blends. However, according to Fig. 3, we find a significant absorbance in both blends in this spectral range. This absorbance may be attributed to the gradual changes in the refractive index in this range. It is known that graded optical constants can have better anti-reflection properties [28, 29].

According to Fig. 4, the J_{sc} is found to be maximum at two thicknesses; about 75 nm and 220 nm in the P3HT:PCBM blend, which means that there are two possible thicknesses at which one can expect to produce the optimal J_{sc} in this OSC. However, it may be important to note that the influence of charge carrier recombination is not considered in this simulation. It is well established that both the absorption as well as recombination increase with the thickness [19] and hence a thickness of 220 nm may be considered to be too thick to get the minimal recombination and hence maximum J_{sc}. Therefore, one may expect a thickness of 75 nm to be the optimal for this BHJ OSC. It is interesting to note that experimentally also a higher J_{sc} is observed at a thickness of 220 nm but the increase is not proportional with the thickness. This may be attributed to the higher recombination and therefore, if one chooses the thickness of 220 nm then this will require relatively a large amount of material without getting much gain in the photocurrent.

Likewise, the plot of J_{sc} in Fig. 5 for PTB7:PCBM shows that the optimal thickness is about 115 nm. This value agrees reasonably well with the 110 nm reported experimentally in [27]. The thicker active layer of PTB7:PCBM blend needed for maximum photocurrent could be due to the ordered packing of PTB7 which allows charge transport over longer distances [27]. For this OSC also one may discard the higher optimal thickness of more than 200 nm due to the reason stated above.

It may be noted that in both Figs. 4 and 5, J_{sc} has been simulated using Ag as cathode as well, which gives slightly higher J_{sc} than using Al without any change in optimal thickness of the active layer. It may also be desirable here to address the issue of the optimal thickness of the cathode using Figs. 6 (a) and (b) for the two OSCs considered here. Accordingly, the J_{sc} in both OSCs does not change by increasing the thickness of Al cathode beyond 40 nm, which may be considered to be the thickness of the cathode to get the optimal performance.

5. Conclusions

We have applied OAAM to simulate the optimal thicknesses of the active organic layer and Al cathode layer in P3HT:PCBM and PTB7:PCBM BHJ OSCs. The optimal thicknesses thus obtained are 75 nm and 115 nm for P3HT:PCBM and PTB7:PCBM active layers, respectively, which agree well with observed ones. Our analysis reveals that PTB7:PCBM will require thicker active layer material compared to P3HT:PCBM for higher J_{sc}. The J_{sc} is maximum when the thickness of Al cathode is 40 nm from the simulation. It is expected that the present results may provide pre-fabrication information for the choice of the thicknesses of the active layer and Al cathode in these OSCs to achieve optimal photovoltaic performance.

Acknowledgements

Authors would like to thank Furong Zhu for discussion on OAAM and providing the optical constants of (PEDOT:PSS), and PTB7:PCBM. David Ompong is supported by the Prestigious International Research Training Scholarship (PIRTS) and University Postgraduate Research Scholarship (UPRS) from Charles Darwin University, Northern Territory, Australia.

References

1. Z. He, B. Xiao, F. Liu, H. Wu, Y. Yang, S. Xiao, C. Wang, T. P. Russell, and Y. Cao, Nature Photon **9**, 174(2015).
2. M. R. Narayan and J. Singh, Journal of Applied Physics **114**, 073510 (2013).
3. D. Ompong, and J. Singh, A European Journal of Chemical Physics and Physical Chemistry **16**, 1281 (2015).
4. J. Mayer, B. Gallinet, T. Offermans, and R. Ferrini, Optics Express **24**, A358 (2016).
5. L. Lu, T. Zheng, Q. Wu, A. M. Schneider, D. Zhao, and L. Yu, Chemical Reviews **115**, 12666 (2015).
6. D. Ompong, and J. Singh, Frontiers in Nanoscience and Nanotechnology **2**, 43 (2016).
7. C. J. Brabec, S. Gowrisanker, J. J. M. Halls, D. Laird, S. Jia, and S. P. Williams, Advanced Materials **22**, 3839 (2010).
8. M. Stolterfoht, A. Armin, S. Shoaee, I. Kassal, P. Burn, and P. Meredith, Nature Communications **7**, 11944 (2016).
9. M. R. Narayan, and J. Singh, *Excitonic and Photonic Processes in Materials* (Springer, Singapore, 2015).
10. M. Niggemann, M. Riede, A. Gombert, and K. Leo, Physica status solidi (a) **205**, 2862 (2008).
11. Z. Tang, W. Tress, and O. Inganäs, Materials Today **17**, 389 (2014).
12. P.G. O'Brien, N. P. Kherani, A. Chutinan, G. A. Ozin, S. John, and S. Zukotynski, Advanced Materials **20**, 1577 (2008).
13. W.-R. Wei, M.-L. Tsai, S.-T. Ho, S.-H. Tai, C.-R. Ho, S.-H. Tsai, C.-W. Liu, R.-J. Chung, and J.-H. He, Nano Letters **13**, 3658 (2013).
14. M. Agrawal and P. Peumans, Optics Express **16**, 5385 (2008).
15. J.-D. Chen, C. Cui, Y.-Q. Li, L. Zhou, Q.-D. Ou, C. Li, Y. Li, and J.-X. Tang, Advanced Materials **27**, 1035 (2015).
16. *Reference Solar Spectral Irradiance: Air Mass 1.5*, http://rredc.nrel.gov/solar/spectra/am1.5/.
17. H. A. Macleod, *Thin-Film Optical Filters* (Taylor and Francis, Hoboken, 2010).
18. F. Zhu, Frontiers of Optoelectronics **7**, 20 (2014).
19. P. Stulik, Designing Amorphous Silicon Solar cells for their optimal photovoltaic Performance (Northern Territory University, Darwin, 1998).
20. J. A. Berning and P.H. Berning, Journal of the Optical Society of America **50**, 813 (1960).
21. J. Gjessing, E.S. Marstein, and A. Sudbø, Optics Express **18**, 5481 (2010).
22. *Optical Data from Sopra SA*, http://sspectra.com/sopra.html.
23. *Optical constants*, https://www.jawoollam.com/resources/ellipsometry-

tutorial/optical-constants.
24. F. Monestier, J.-J. Simon, P. Torchio, L. Escoubas, F. Flory, S. Bailly, R. de Bettignies, S. Guillerez, and C. Defranoux, Solar Energy Materials and Solar Cells **91**, 405 (2007).
25. These optical constants were made available, courtesy of Prof. Furong Zhu.
26. Z. Kam, Q. Yang, X. Wang, B. Wu, F. Zhu, J. Zhang, and J. Wu, Jishan, Organic Electronics **15**, 1306 (2014).
27. Y. Zheng, T. Goh, P. Fan, W. Shi, J. Yu, and A. D. Taylor, American Chemical Society Applied Materials & Interfaces **8**, 15724 (2016).
28. Y. Zhang, W. Cui, Y. Zhu, F. Zu, L. Liao, and S. T. Lee, B. Sun, Energy & Environmental Science **8**, 297(2015).
29. S. F. Rowlands, J. Livingstone, and C.P. Lund, Solar Energy 76, 301 (2004).